Higher-order effects and validity of the point-dipole approximation for conjugated extended molecular emitters near plasmonic nanostructures

Mhamad Hantro[a)], Bjorn Maes[b)], Gilles Rosolen[b)], Colin Van Dyck[a)]*
[a)]Theoretical Chemical Physics Group, Research Institute for Materials Science and Engineering, University of Mons, 20 Place du Parc, 7000 Mons, Belgium.
[b)]Micro- and Nanophotonic Materials Group, Research Institute for Materials Science and Engineering, University of Mons, 20 Place du Parc, 7000 Mons, Belgium.
[*]Corresponding author: Colin.VanDyck@umons.ac.be

Abstract: Rapid advancements in nanotechnology have allowed for the characterization of single molecules, by placing them in the vicinity of nanoplasmonic structures that are known to confine light to sub-molecular scales. In this study, we introduce a theoretical framework that captures higher-order effects, and we explore the limits of the standard description of a molecular emitter as a point-dipole. We particularly focus on the role played by the emitter chain length and the electron conjugation. Strong deviations are observed from the point-dipole approximation, which demonstrates that higher order effects are essential to fully capture the emission rate of extended molecules in the vicinity of nanoparticles. This deviation strongly depends on the orientation of the conjugated chain versus the nanoplasmonic structure. Finally, we propose a simple rationalization that qualitatively assesses the difference from the point-dipole approximation.

Keywords: plasmonics, electron conjugation, TD-DFT, higher-order effects, point-dipole approximation, Purcell enhancement

I. Introduction

The point-dipole approximation (PDA) has long been used in the domains of quantum chemistry[1], photonics, solids, and many others[2–4]. It consists of approximating an extended oscillating density as an oscillating point dipole. It usually provides a reasonable approximation, and its simplicity offers a path to qualitatively understand various physical phenomena. Over the past two decades, rapid advancements in the field of nanotechnology have enabled unprecedented confinement of electromagnetic fields,

especially through plasmons, in open-system cavities [5–12]. These systems gave access to an unprecedented degree of molecular probing, enabling single-molecule localization[10,13–16], and sub-molecular characterization[7,14,17,18]. This consequently requires a realistic description of quantum emitters, beyond the point-dipole approximation, as has been exemplified in several recent studies[19–27].

In the literature, the effect of the emitter-plasmon interaction has been shown to trigger different effects, depending on the interaction strength[19,28–30]. In this study, the weak-coupling regime is assumed, meaning that the interaction is considered as a weak perturbation, while the wavefunction is not perturbed by the vacuum electromagnetic field. Within these assumptions, the rate is obtained with Fermi's golden rule[31,32]. The latter leads to the well-known Purcell spontaneous rate enhancement effect. While all excited states of emitters have a natural vacuum spontaneous rate, this rate is modified by the local density of electromagnetic states (LDOS) within the spatial extent of the transition density of the emitter. Purcell factors of several orders of magnitude[33] can be reached within nanoplasmonic structures.

In free space, the wavelength of the emitted light tends to be several orders of magnitude larger than the dimensions of the emitter, thus the emitted light can be seen as temporally and spatially coherent across the emitter. This constitutes the working hypothesis behind the PDA. However, high confinements of the electromagnetic field are observed in plasmonic nanostructures, which shrink the effective wavelength toward the nanometer scale[34]. This challenges the PDA hypothesis, and it becomes necessary to establish its bounds of validity. This appears especially essential as molecular emission in the visible range usually requires using conjugated molecular chains, in which excitons can delocalize over a few nanometers[35]. This important class of emitters can be found in many applications triggered by emitter-plasmon interactions, covering organic light-emitting diodes[36,37], tip/surface-enhanced Raman spectroscopy, electrically driven single-photon sources[10,11,17], and molecule-based quantum-optical devices[18,23,38]. Interestingly, a breakdown of the PDA translates into the observation of higher-order effects. This has been suggested as a way to reveal and exploit the dark dipole-forbidden transitions of quantum emitters[34].

In this paper, we first introduce a newly developed mode-expansion-based method[21] that can be used to study molecular emitters while taking into account their spatial extension, and the high-order transition modes beyond dipolar effects. This method solves the full Maxwell equations and does not rely on the quasi-static approximation which has been used in several previous studies[19,23]. It is then used to assess the validity of the PDA, for two different conjugated molecular emitters, near two different types of plasmonic structures (section III). First, we consider the free-base phthalocyanine (H_2Pc) molecule placed in a tip-substrate nanogap. Second, we characterize oligothiophenes of different chain lengths placed in the vicinity of a gold nanosphere. Interestingly, we observe a failure of the PDA in conjugated systems, with significant overestimation, or underestimation, of the emission rate. These findings are consistent with previous studies on higher-order effects in plasmonic environments[19,23]. This validates the introduced theoretical framework. In the present work, we further report a significant dependence of higher-order effects on the orientation and displacement of the molecular emitter. Moreover, we show that increasing the chain length of conjugated molecular compounds promotes larger deviation from the point-dipole behavior. We rationalize this observation by probing the spatial dependence of the LDOS at the scale of the emitter. Interestingly, we argue that the large deviation would originate from octupolar and/or interfering cross terms within a multipolar development picture, which are often neglected in molecular luminescence studies.

II. Methods

Within the nonrelativistic regime, the light-matter interaction can be described[34] using the minimum coupling Hamiltonian. In the weak coupling regime, and neglecting both the nonlinear ponderomotive term and the spin-term[34,39], Rivera et al. showed that the perturbative decay rate Γ of a molecular emitter in a dissipative medium can be given by Fermi's golden rule[34]:

$$\Gamma = \frac{2\pi}{\hbar^2}\frac{e^2\hbar}{\pi\varepsilon_0 c^2}\int d\mathbf{y}\sum_k \frac{\omega_0^2}{c^2} Im\,\varepsilon(\mathbf{y})\left|\left\langle e\right|\sum_\alpha \frac{G_{ik}p_i}{m_e}(\mathbf{r}_\alpha,\mathbf{y},\omega_0)+\sum_\beta \frac{G_{ik}p_i}{m_\beta}(\mathbf{R}_\beta,\mathbf{y},\omega_0)\left|g\right\rangle\right|^2 \quad \textbf{(1)}$$

where $|g\rangle$ and $|e\rangle$ refer to the ground and excited states of the molecular emitter, and $\overleftrightarrow{G}$ is the Green tensor of the Maxwell equations solved for the enhancing medium. The

sum over k represents the sum over the three directions, **y** is the field sources' positions, ε is the electric permittivity, ω_0 is the emitter's angular frequency, $\hbar$ is the reduced Planck constant, e is the elementary charge, c is the speed of light in vacuum, $m_{e(\beta)}$ is the mass of an electron (nucleus), and p_i is the i[th] component of the linear momentum operator. The α (β) - summations are over all the N_α (N_β) electrons (nuclei) with coordinates $\mathbf{r}_\alpha$ ($\mathbf{R}_\beta$). To compute the rate, it is necessary to solve the Maxwell equations to obtain the Green tensor and the Schrödinger equation for the emitter states.

The emitter is described by the usual molecular Hamiltonian, within the Born-Oppenheimer approximation of the wavefunction as a product $\psi(\mathbf{x}_\alpha)\chi(\mathbf{R}_\beta)$, where $\mathbf{x}_\alpha$ are the electron spin-coordinates. Consequently, the nuclei summation vanishes because of the orthogonality of the e and g electronic states. Noteworthy, we neglected the Franck-Condon factor and the parametric dependence of the electronic wavefunction with nuclei coordinates (known as the Condon approximation). Following[34] by introducing a Green tensor identity and developing the squared bracket as a product of two integrals involving a one-body operator, we obtain:

$$\Gamma = \frac{2\pi}{\hbar^2}\frac{e^2\hbar}{\pi\epsilon_0 m_e^2 c^2} N_\alpha^2 \int\int d\mathbf{x}_\alpha d\mathbf{x}_\alpha{}' \; \psi_e^*(\mathbf{x}_\alpha)\psi_e(\mathbf{x}_\alpha{}')\left(\mathrm{Im}\,\mathrm{G}_{ij}(\mathbf{r},\mathbf{r}',\omega_0)\right)\left(p_j\psi_g(\mathbf{x}_\alpha)\right)\left(p_j^*\psi_g^*(\mathbf{x}_\alpha{}')\right), \qquad \textbf{(2)}$$

where **r** and **r'** are the spatial coordinates of an arbitrary electron in the system and the integrals are done over all electron spin-coordinates, $\mathbf{x}_\alpha$. Also, we did not consider how the dielectric response of the plasmonic environment may affect the excitation properties of the molecule. Indeed, this has been reported as negligible in a previous study[26].

The Green tensor is obtained in this study using a GEneralized NOrmal Modes Expansion (GENOME) based on eigenpermittivity modes, where each mode m is characterized by a permittivity eigenvalue associated with a field profile $\mathbf{E}_m$, as was introduced in a previous study[40]. Usually, the mode expansion is performed with eigenfrequency modes (or quasinormal modes), where the resonance frequencies of the cavity with a fixed permittivity ε_i are the eigenvalues of the problem. However, eigenfrequencies are global properties of the system and for open systems, as it is the

case here, they are complex, leading to a laborious mode normalization procedure that requires significant expertise[41,42]. On the contrary, the eigenpermittivity mode set refers to a closed volume (the scatterer), offering the advantage of simple normalization. The modes are defined at a fixed frequency (the emission frequency of the emitter), and their corresponding eigenvalues ε_m constitute a permittivity set. Moreover, they are orthogonal and form a complete set[40,43].

We inject the GENOME expansion of the Green tensor in Eq. (2), as was recently done[21] and we assume from this point that the electronic wavefunction is developed in a real LCAO basis set. We find:

$$\Gamma = \Gamma_0 + \frac{2}{k^2}\frac{e^2\hbar}{\varepsilon_0 m_e^2 c^2}\sum_m \mathrm{Im}\left[\zeta_m\left(N_\alpha \int d\mathbf{x}_\alpha \psi_e(\mathbf{x}_\alpha)\mathbf{E}_m(\mathbf{r})\boldsymbol{\nabla}_\mathbf{r}\psi_g(\mathbf{x}_\alpha)\right)^2\right], \quad \textbf{(3)}$$

where k is the wavevector, $\mathbf{r}$ is the position of one electron, ζ_m are expansion coefficients which depend on the mode eigenvalue[21] and Γ_0 is the decay rate of the emitter considering only $\overleftrightarrow{G}_0$, the background medium Green tensor in Eq. (2). The second contribution associates with modes of the scatterer, *i.e.*, the tip or the sphere in the following. For multilayer structures, $\overleftrightarrow{G}_0$ can be obtained analytically[44]. However, it has been shown that the point dipole approximation is reasonably accurate for large emitters separated by 0.5 nm from a gold nanoparticle of radius larger than 50 nm[20]. Here, the molecule is placed at a minimum distance of 1 nm from the flat air/metal interface, so Γ_0 has been calculated within the point dipole approximation.

Eq. (3) can be rewritten using the spinless transition density[45] $\rho_{ge}(\mathbf{r},\mathbf{r}')$ instead of the full electronic wavefunction. Then, it becomes a simple three-dimensional integration:

$$\Gamma = \Gamma_0 + \frac{2}{k^2}\frac{e^2\hbar}{\varepsilon_0 m_e^2 c^2}\sum_m \mathrm{Im}\left[\zeta_m\left(\int d\mathbf{r}\left[\mathbf{E}_m(\mathbf{r})\boldsymbol{\nabla}_\mathbf{r}\rho_{ge}(\mathbf{r},\mathbf{r}')\right]_{\mathbf{r}'=\mathbf{r}}\right)^2\right], \quad \textbf{(4)}$$

where:

$$\rho_{ge}(\mathbf{r},\mathbf{r}') = N_\alpha \int ds_1 d\mathbf{x}_2 \ldots d\mathbf{x}_N \psi_g(\mathbf{r}, s_1, \mathbf{x}_2, \ldots, \mathbf{x}_N)\psi_e(\mathbf{r}', s_1, \mathbf{x}_2, \ldots, \mathbf{x}_N),$$

in which s_1 is the spin variable of the first electron. These are general formulas in which the transition density can be evaluated using the usual quantum chemistry techniques. In this paper, we use the linear response TD-DFT formalism to describe the molecular emitter. Consequently, the transition density can be constructed from two rectangular transition density matrices $X_{\mu\nu}$ and $Y_{\mu\nu}$ relating occupied (φ_μ^{occ}) and virtual (φ_ν^{virt}) canonical single-electron Kohn-Sham orbitals. It is given by the sum[46–48]:

$$\rho_{ge}(\mathbf{r},\mathbf{r}') = \sum_{\mu}^{N_{occ}} \sum_{\nu}^{N_{virt}} \varphi_\mu^{occ}(\mathbf{r}) X_{\mu\nu} \varphi_\nu^{virt}(\mathbf{r}') + \sum_{\mu}^{N_{occ}} \sum_{\nu}^{N_{virt}} \varphi_\nu^{virt}(\mathbf{r}) Y_{\mu\nu} \varphi_\mu^{occ}(\mathbf{r}'), \qquad \textbf{(5)}$$

where the first term corresponds to excitation and the second term to deexcitation processes. A more compact version is achievable using the two unitary transformations provided by the singular value decomposition of each matrix. The singular vector pairs, θ_i^{elec} and θ_i^{hole}, are commonly named Natural Transition Orbitals (NTO) in the literature[47,49]. In these specific sets, the transition density transforms into single sums over electron-hole excitation and de-excitation orbital pairs:

$$\rho_{ge}(\mathbf{r},\mathbf{r}') = \sum_{i}^{N_\alpha/2} \left[\sqrt{\lambda_{i,X}}\theta_i^{X,elec}(\mathbf{r})\theta_i^{X,hole}(\mathbf{r}') + \sqrt{\lambda_{i,Y}}\theta_i^{Y,hole}(\mathbf{r})\theta_i^{Y,elec}(\mathbf{r}')\right], \qquad \textbf{(6)}$$

where $\sqrt{\lambda_i}$ are the singular values of $X_{\mu\nu}$ and $Y_{\mu\nu}$ matrices. The sum of all λ_i must be equal to one (in case de-excitation terms are present, the identity becomes $\sum_i \lambda_{i,X} - \lambda_{i,Y} = 1$) and the development is generally largely dominated by one singular value close to one for molecular emitters[49]. As $\mathbf{r}$ and $\mathbf{r}'$ coordinates separate into the TD-DFT transition densities, we can introduce the velocity transition density $\gamma_{ge}(\mathbf{r})$, and rewrite Eq. (4) as:

$$\Gamma = \Gamma_0 + \frac{2}{k^2}\frac{e^2\hbar}{\varepsilon_0 m_e^2 c^2}\sum_m \mathrm{Im}\left[\zeta_m \left(\int d\mathbf{r}\, \mathbf{E}_m(\mathbf{r})\, \gamma_{ge}(\mathbf{r})\right)^2\right], \qquad \textbf{(7)}$$

where

$$\gamma_{ge}(\mathbf{r}) = \sum_{i}^{N_\alpha/2} \left[\sqrt{\lambda_{i,X}}\nabla_{\mathbf{r}}\theta_i^{X,elec}(\mathbf{r})\theta_i^{X,hole}(\mathbf{r}) + \sqrt{\lambda_{i,Y}}\nabla_{\mathbf{r}}\theta_i^{Y,hole}(\mathbf{r})\theta_i^{Y,elec}(\mathbf{r})\right]. \qquad \textbf{(8)}$$

Concretely, we use the linear response TD-DFT method as implemented in the Gaussian 16 quantum chemistry software using the CAM-B3LYP[50] hybrid functional[51]. The

molecular structures are optimized in their first electronic excited state as we are interested in emission properties. In supplementary material (section S4.1), we explain how the X and Y matrices are constructed from the Gaussian output and how the NTO functions are developed in the LCAO Gaussian basis set. The LCAO development of the NTOs is directly injected into Eq. (8) to evaluate the transition density on the integration mesh. Noteworthy, all the derivatives are calculated analytically using the definition of each gaussian basis function.

In the Gaussian input, we use the 6-31g(d,p) basis set for the three considered oligothiophene chains: an α-bithiophene (2T), an α-quaterthiophene (4T), and an α-sexithiophene (6T). For the H_2Pc molecule, we use a heavier basis set 6-311++g(d,p) to achieve a better convergence of the emission wavelength. The rate integration is performed on a uniform rectangular grid with equal spacing along the 3 axes of the molecule of 2 points per Bohr. To check the validity of our numerical procedure, we use this integration mesh and the NTO development to calculate the transition dipole moments of the molecules. Comparing these to Gaussian's output, we find the errors on transition dipole moments to be 5%, 2.58%, 1.51%, and 1.07% for the 2T, 4T, 6T, and H2Pc respectively. The error on 2T gets reduced even further with a finer mesh of 4 points per Bohr down to 0.5%. The mesh is thus the main source of numerical error. As it significantly increases the computational resources needed, we keep this parameter to 2 points per Bohr in every further calculation.

This theoretical framework captures all the multipolar higher-order effects, beyond the PDA approximation. Indeed, these are directly included as the Green tensor gets integrated over the whole transition density. Interestingly, the Green tensor can be developed into multipoles (see supplementary material section S5). Doing so, it is shown that the framework contains all multipolar higher-order terms, including interference terms among orders, as well as the higher-order magnetic transitions. Having discussed the way to calculate the perturbative decay rate of an extended molecular emitter in a dissipative medium, we compare it to a point-dipole rate. The point-dipole rate calculation was carried out by integrating the Poynting vector on the surface of a sphere englobing it. The power ratio of the dipole rate in the nanostructure

and in vacuum gives the Purcell enhancement. This is done using the Frequency Domain study in the RF-Module of COMSOL Multiphysics® software with the smallest mesh element equal to 0.5 Angstrom for the tip (mainly around the protrusion), and 1 Angstrom for the nanosphere. Permittivities of Gold and Silver were obtained from the Johnson-Christy dataset[52].

III. Results and discussion

A) H2Pc in a plasmonic tip-substrate nanogap

As a first step, we focus on the H2Pc molecule placed on a silver substrate and approached by a silver STM (Scanning Tunnelling Microscope) tip. This system has been studied experimentally, offering detailed photon intensity and linewidth maps of the emitter that provide valuable insights on the Purcell enhancement [23,53]. The molecular emitter gets excited from inelastic scattering of tunneling electrons in the molecule, and the emission rate is enhanced by the plasmonic environment. H_2Pc is a conjugated molecule in which the transition density and NTO orbitals significantly extend over the whole molecular backbone, as can be observed in Fig. 1b, making it a good candidate to investigate the PDA validity. Fig. 1a shows the geometry of the plasmonic environment used in the COMSOL simulation, with the parameter set used to model the STM tip as a nanorod with a small protrusion. The small protrusion was added by merging a 1 nm diameter sphere with the nanorod and adding a fillet of radius 0.1 nm at contact edges, which avoids sharp edges. We note that classical simulations of the EM field distribution were proven valid in the presence of atomistic protrusions, when compared to full quantum level simulations[54]. We optimize the length of the rod to reach the dipolar plasmonic resonance of the system at the emission wavelength (652 nm) – see supplementary material section S1.1. Interestingly, we also simulated a larger tip with protrusion model, as introduced in a previous work[24,26,27]. This did not modify our main conclusions, and thus we report it here as supplementary material (section S3).

The experimental spacer between the molecule and the substrate was not explicitly accounted for in the simulation. This is because a thin dielectric layer would only shift the resonance frequency of the STM tip[55] and thus simply require a slight modification of the tip dimension to resonate with the emitter wavelength. Hence,

we implicitly consider the spacer by placing the closest molecular atom at a minimal distance of 1 nm from the substrate in every calculation. Note also that for the PDA calculation, we place the point-dipole at the center of mass of H_2Pc, which in this case is the center of symmetry as well.

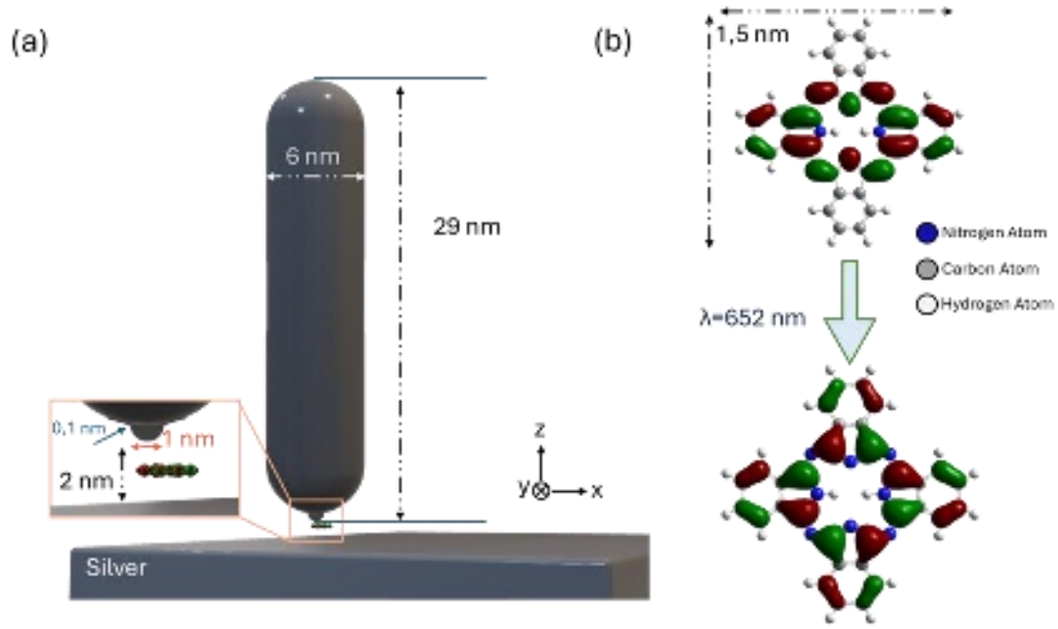

Figure 1*: **STM tip scanning an H2Pc molecule.** a) Tip geometry and dimensions used in the COMSOL simulation of the plasmonic environment. b) Main NTO pair representing the electronic transition in the H_2Pc molecule with emission wavelength as predicted by TD-DFT calculations.*

We first report the rate maps calculated for the molecule lying flat 1 nm above the substrate in Fig. 2a. The top panel shows the map calculated using our method for the molecular emitter. The bottom panel shows the map calculated for the molecule when it is approximated as a point-dipole (PDA). The molecule is translated over the substrate (scanning the xy-plane) while having its dipole moment oriented parallel to the surface, in the x direction. We note that the transition dipole of H2Pc is oriented along the two H atoms lying at the center of the molecule. Qualitatively, the PDA map (Fig. 2a, bottom) is in line with the full molecule map (Fig. 2a, top). The two bright spots thus originate from the enhanced field distribution around the tip and not from a brighter

position within the molecular substructure. This profile aligns closely with the experimental observation obtained for H2Pc molecule placed in a tip-substrate nanogap[23]. Moreover, the line broadening due to the Purcell effect, defined as $\Delta E = \hbar\Gamma$ [31], shows a peak-to-valley difference of 1.35 meV (maximum of 1.35 meV at the hotspot, and a minimum of 3×10^{-5} meV away from the tip). This predicted broadening follows closely the experimental findings, with the lower calculated value likely resulting from the wider tip-substrate gap in our model, which leads to an overall reduced confinement.

From a finer comparison perspective, we observe that the full molecular enhancement map shows less saturated colors. This indicates a weaker overall enhancement for the full molecular rate calculation. A quantitative comparison is available in Fig. 2b with profile curves of the Purcell enhancement across the two bright spots (dashed lines in Fig. 2a). First, we see that the PDA overestimates the rate by an amount of up to 25%. Such discrepancy can be attributed to the molecular extension, which probes the field over a larger volume, as opposed to a point dipole, which probes the field at a specific location. Further characterizations following this qualitative picture are given at the end of Section III B. A second difference lies within the shift of the peak position of 0.2 nm, which is non-negligible as it is about a tenth of the molecular length (~ 2 nm as indicated in Fig. 1b).

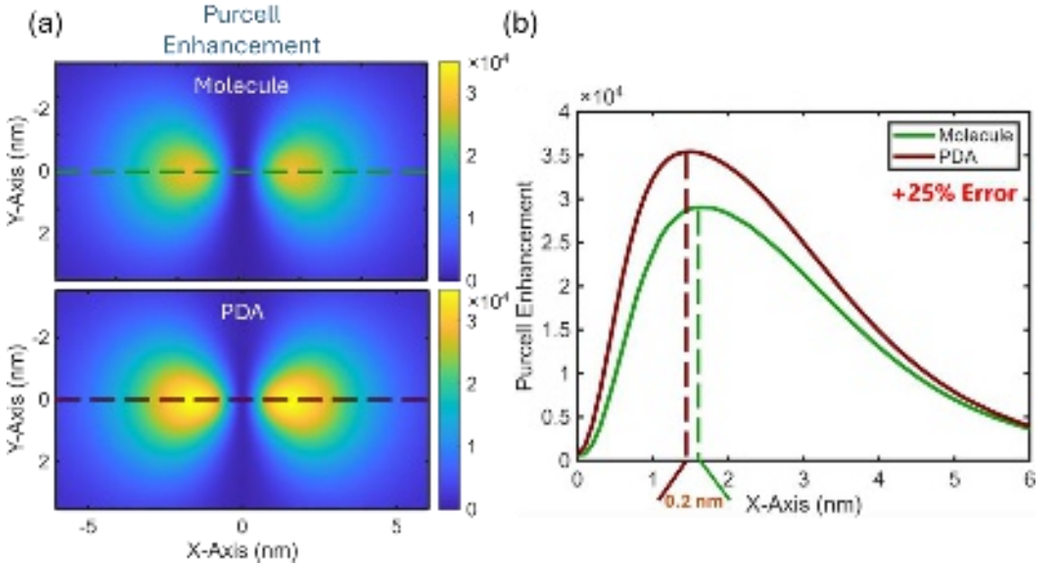

Figure 2*: **Differences between full molecule Purcell enhancement and PDA.** a) Maps of the Purcell enhancement of the H2Pc molecule inside the gap at different positions in the xy plane. Top (bottom) panel represents the full (PDA) molecular rate. b) Purcell enhancement along a line cut that crosses the center of the two lobes, as represented by the dashed lines in panel (a). Because of symmetry, only the positive x-axis is represented.*

To further understand the deviation from the PDA, Fig. 3 reports the effect of vertically moving the molecule within a larger gap of 4 nm. Note that the rod length has been re-optimized to a length of 30 nm (the gap size affects the plasmonic peak position) in order to maintain the dipole resonance of the tip at the emitter wavelength (see supplementary material section S1.1). The molecule is sitting with its center at a lateral distance of 1.7 nm from the tip center, where the Purcell enhancement is at maximum. Both PDA and full molecule Purcell enhancements increase rapidly with decreasing molecule-tip distance (increasing z-position measured from the substrate). Three nanometers away from the tip, the PDA overestimates the molecule by about 12%. This error increases at closer distances, reaching about 15% at one nanometer of the tip extremity. This shows that the local field variations limiting the validity of the PDA are stronger near the tip structure.

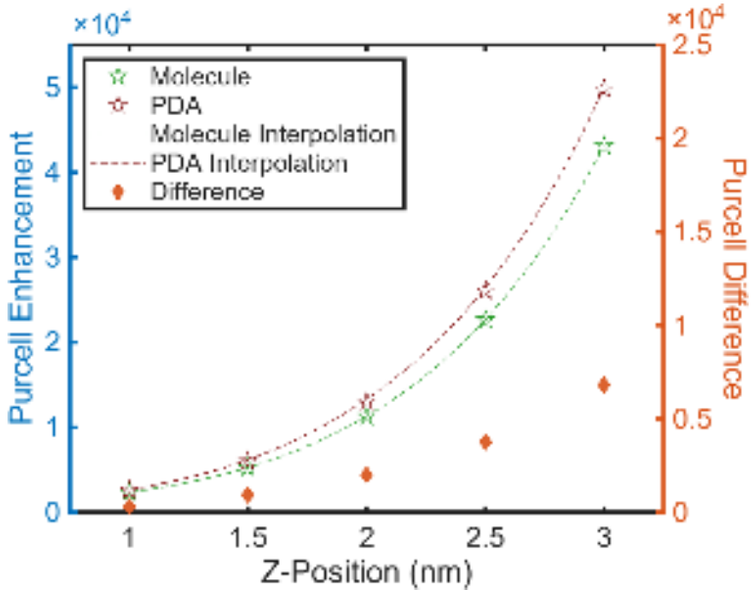

Figure 3*: **The PDA deviation is stronger for a molecule closer to the tip.** The effect on the Purcell enhancement of vertically shifting the molecule inside the nanogap. The*

H_2Pc molecule is lying flat in a 4 nm nanogap and moved from a 1 to 3 nm distance away from the substrate. The Purcell enhancements are indicated with star markers, while the absolute error difference is indicated by rhombuses.

B) <u>Oligothiophene chains near a plasmonic nanosphere</u>

In the previous section, we observed significant deviations from the PDA for H_2Pc emitters. We consider this feature a direct consequence of the delocalized nature of electronic excitations involving π-orbitals. This is well observable within the NTO structure of Fig. 1b. To further characterize the interplay between the PDA and electronic conjugation, we focus here on oligothiophene chains. These highly conjugated chains are known to exhibit large π-orbital delocalization, up to 7 nm[35]. Moreover, this delocalization is highly directional which translates into transition dipoles that are well aligned along the molecule backbone. These features can directly be observed in the NTO reported in Fig. 4. We focus here on three different chain lengths with oligomers made of two, four and six repeated thiophene units. The respective chain lengths of the oligomers are 0.85, 1.6 and 2.4 nm.

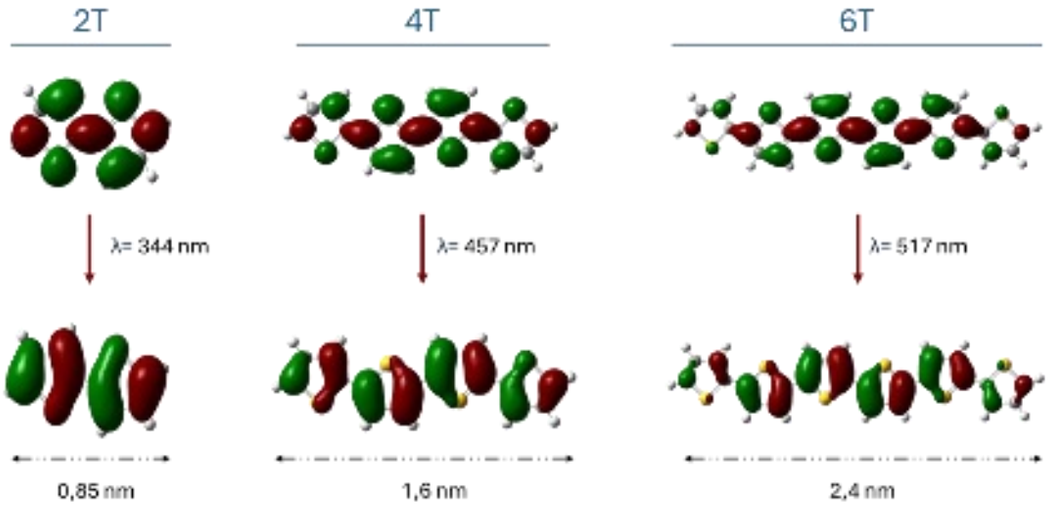

Figure 4*: Oligothiophene transitions representing the most contributing NTO pair, together with the corresponding transition wavelength. Below is indicated the length of each structure.*

The leftmost sketches in Fig. 5 show the different studied setups of a molecule near a gold nanosphere of 5 nm radius. This system was chosen to illustrate the importance of

higher-order effects even for configurations that have not been specifically designed to reinforce the field confinement. Notably, such system radiates in the far-field as the emitter couples mainly with a dipolar mode of the nanosphere (see the individual modal contribution analysis to the full Purcell enhancement in the supplementary material). We note that the experimental setup can be adapted to optimize the far-field emission[56]. Furthermore, the latter system supports a plasmonic peak in optical response centered around 500 nm and with a long tail toward the UV, enabling all three molecules to effectively couple to the dipolar plasmonic mode of the nanosphere (see supplementary material section S1.2). We focus on calculating the Purcell enhancement of the spontaneous emission, assuming that the emitters are already in their relaxed excited state. Different configurations of the emitter's positions and orientations are simulated with a specific focus on identifying the limits of the PDA. In each configuration we ensure that the atom of the emitter that is the closest to the surface always lies at a minimal distance of 1 nm.

First, in Fig. 5a, the molecule is placed in the tangent plane with its center passing through the axis of symmetry of the nanosphere. The molecule, initially at a 1 nm distance from the gold nanosphere surface, is shifted radially away from the sphere. The three plots on the right part of Fig. 5a show the results for molecules 2T, 4T and 6T respectively. The relative error, written within the graph, increases with the size of the molecule from 10% to 70%. The PDA validity is restored again for surface-molecule distances roughly equal to the molecular length. This suggests that the PDA starts to break for distances that are smaller than the emitter length, a rule of thumb that was stipulated in a previous theoretical study[20].

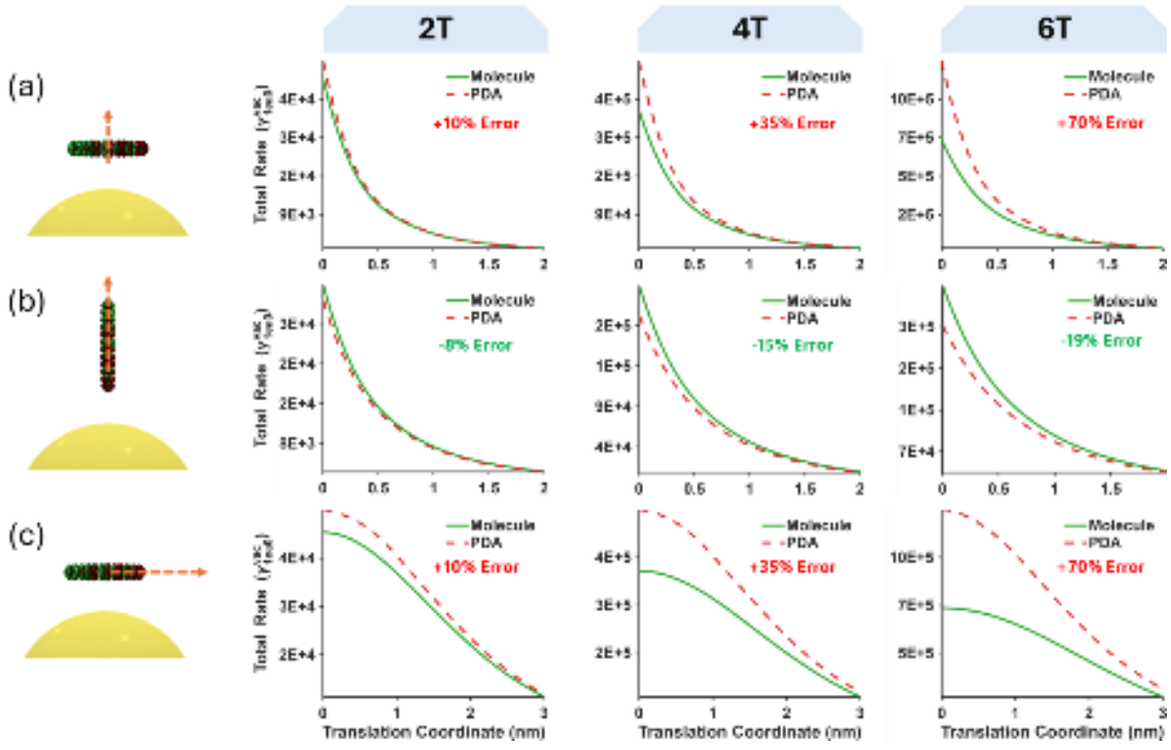

Figure 5*: **Influence of molecule orientation and size on the Purcell enhancement for the full molecule and the PDA**. Studied cases represented in the leftmost sketches are a) radial shift of the tangent molecule, b) radial shift of the normal molecule, c) lateral shift of the tangent molecule. The orange arrow indicates the direction of translation. A positive (negative) error sign indicates that the PDA overestimates (underestimates) the rate's enhancement. The error is reported for the case of zero translation.*

Second, in Fig. 5b, we modify the orientation of the molecule and align the conjugated long axis in the radial direction of the nanosphere. In the same line as before, we probe the influence of the distance between the emitter and the gold surface. The initial distance is set for the configuration with the atom closest to the sphere at a 1 nm distance. Then, the three molecules are translated radially away, and the corresponding plots are reported. For this specific orientation, we see an opposite trend with the PDA underestimating the emission rate. Again, for translations about the emitter length the PDA rate is recovered, and the approximation becomes valid.

Third, in Fig. 5c, we explore the influence of the molecule displacement in the tangent configuration. Interestingly, the recovery of the PDA is much slower for translations in this direction. This shows that the large PDA breaking that we observe in Fig. 5a for the tangent orientation of the molecule is a solid feature. It remains preserved for significant lateral displacements. Qualitatively, this seems acceptable as the left part of the molecule remains exposed to the nanosphere upon translation.

Naturally, it is possible to rationalize any deviations from the PDA by considering the higher-order terms of the multipole expansion. On the other hand, it is not straightforward to anticipate at which order an accurate rate would be recovered. Several studies pointed toward the important role played by the quadrupolar transition moment, which gets enhanced by the large field gradients existing around plasmonic structures[34,57,58]. Interestingly, the integration of the TD-DFT transition density to calculate the quadrupolar and octupolar transition moments (origin at the center of mass of the molecule) shows that the first excited state of oligothiophene chains associates with close to zero quadrupolar moments, and large octupoles (see supplementary material section S4.2). The magnetic dipole transition moment is also negligible. Moreover, we stress that considering only the point-dipole term of the development overestimates the emission rate for the tangent orientation of the emitter. However, simple addition of the quadrupolar and octupolar contributions of the expansion could only increase the emission rate. Therefore, the breakdown of the PDA can only arise from crossed-interference terms in the multipole expansion, likely involving interferences between dipolar and octupolar moments[59,60] (see supplementary material section S5).

Consequently, a rationalization of the observed results on the basis of higher-order terms is anticipated to be cumbersome. In fact, at a qualitative level, the observations can be understood from a fine analysis of a point-dipole emission rate displaced within the molecular spatial extension. This in turn consists in probing the photonic LDOS around the plasmonic medium. The latter variation is reported in Fig. 6, using a coordinate normalized to the emitter length and an emission rate normalized to the maximal rate computed within the emitter. Panel (a) focuses on the tangent emitter with

the center placed on the symmetry axis of the sphere, the emitter is thus placed at the largest error position of Fig. 5a. For the three chains, the curve goes through a marked maximum, positioned at the center of the emitter. The shortest chain reveals a near-flat normalized enhancement, with a maximum variation of around 8% across the chain. The curvature increases for the two other chains, being larger for the larger emitter. The 6T molecule shows a drastic difference of around 33% across its length. This correlates well with our findings that the maximum PDA deviation was seen for the longest chain. Approximating the molecule as a point-dipole corresponds to considering only the enhancement at its center, which corresponds to a maximum for this setup. Thus, the PDA is expected to overestimate the rate, which agrees with the conclusions obtained for the full rate simulations.

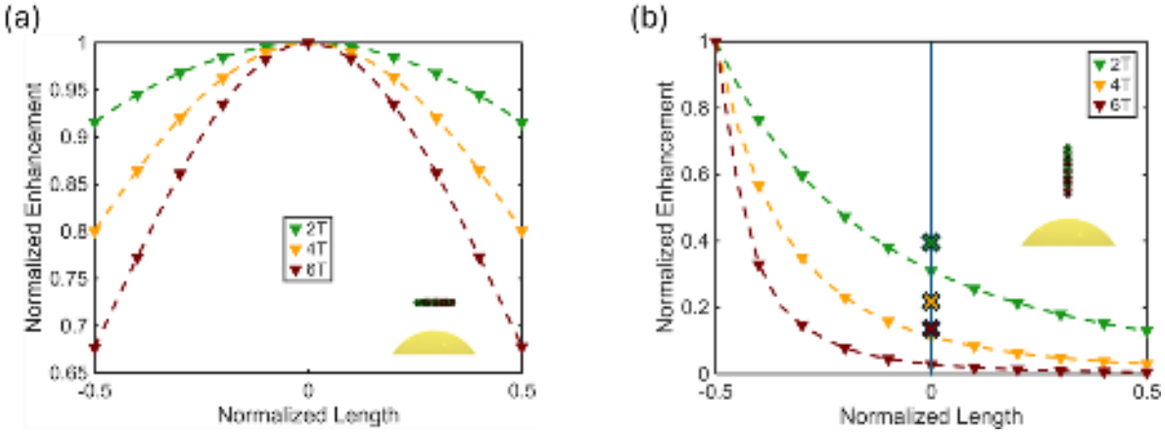

Figure 6*: **Normalized photonic LDOS within the molecule's spatial extension** for a) Centered-Tangent setup, b) Centered-Normal setup. The triangles indicate the normalized enhancement, the dashed lines are guides for the eye, the cross marker is the rate averaged over all the triangles.*

Fig. 6b focuses on the normal emitter with the center placed on the symmetry axis of the sphere. The emitter is placed at the largest error position of Fig. 5b, which is for the molecule edge at 1 nm from the gold surface. A drastic variation (triangle markers) appears across the emitter due to the strong light confinement along this direction. The part that is closer to the nanosphere feels a larger enhancement than the other part. As the PDA corresponds to the rate taken at the center of the molecule, this suggests that the rate is underestimated by the PDA for the lower part, and overestimated for the

upper part, of the molecule. This error balancing may explain why the PDA error is lower for the normal orientation of the emitter, in comparison with the tangent orientation. Along the vertical line at the center of Fig. 6b, we add the average normalized enhancement (cross markers) of the point-dipoles (triangle markers) along the extent of the molecule. The three chains reveal a higher average enhancement value than the enhancement of a point-dipole at the center of the molecule. This agrees with our findings that the PDA underestimates molecular enhancement in this configuration (see Fig. 5b). Furthermore, we can see that the separation of the PDA from the mean value increases with the length of the chain, correlating with a larger error for a larger emitter.

This intuitive reasoning, while not quantitative, agrees qualitatively with our extensive simulations. Such an analysis may be used as a test to anticipate the role played by higher-order effects of highly directional conjugated chains near plasmonic structures. It remains to be tested for other molecular structures in the future.

IV. Conclusions

In this paper we introduce a method to compute the total spontaneous emission rate of extended quantum emitters near nanoplasmonic structures, adapting an existing model for hydrogen[21] to include many-electron photoemitters like molecules. Our model computes the full emission rate, *i.e.*, it includes higher-order transition and interference terms. We validate the model using an H_2Pc molecule in an STM gap, by comparing with previous experimental data[23]. Additionally, we investigate the impact of emitter length, simulating conjugated oligomers near a gold nanosphere, where pronounced higher-order effects invalidate the PDA. Our study points toward a significant role played by interference and octupolar contributions. We show that PDA can underestimate and overestimate the rates (up to 70%), and we observe that the PDA is not accurate if the longest dimension of the molecule exceeds its separation from the scatterer. We finally qualitatively explain the deviation of the PDA with the LDOS variation along the molecule extension. This framework holds promise for application to molecular structures with large quadrupolar moments, particularly with dipole-forbidden transitions. In a nanogap, such "dark" molecules could be induced to emit

light, effectively transforming them into bright emitters. In the future, our framework may also be refined to explicitly compute the radiative rates of the system, providing additional insight beyond the total rates computed here. It will allow the design of nanoplasmonic structures that maximize the radiative rates of usually dark transitions.

Supplementary material

The Supplementary Material consists of five sections. Section 1 presents data on the tuning of plasmonic resonances for both the tip and the gold nanosphere. Section 2 discusses the convergence of our method based on the mode expansion approach, GENOME. Section 3 examines extended tip geometries, demonstrating the consistency of our results. Section 4 outlines the calculation of the velocity transition density using natural transition orbitals, along with numerical values of the multipole moments of the molecules under study. Finally, Section 5 explores the multipolar expansion of the full rate equation.

Acknowledgments

G.R. would like to thank Prof. Yonatan Sivan for his invaluable assistance and insights in the mathematical development and justification of the GENOME method. We also acknowledge CECI (Consortium des Équipements de Calcul Intensif) for providing us with computation time.

Research funding

We acknowledge the support from Actions de Recherche Concertées (project ARC-21/25 UMONS2), FRS-FNRS (PDR project T.0166.20).

Author contributions

M. Hantro conducted the research and performed simulations. B. Maes, G. Rosolen and C. Van Dyck supervised the research. All authors contributed to the manuscript writing.

Conflict of interest

Authors state no conflict of interest.

Data availability statement

The datasets generated and/or analysed during the current study are available from the corresponding author upon reasonable request.

V. References

[1] W.J.D. Beenken, and T. Pullerits, The Journal of Chemical Physics **120**(5), 2490–2495 (2004).
[2] A.B. Evlyukhin, and S.I. Bozhevolnyi, Phys. Rev. B **71**(13), 134304 (2005).
[3] H. DeVoe, The Journal of Chemical Physics **41**(2), 393–400 (1964).
[4] H. DeVoe, The Journal of Chemical Physics **43**(9), 3199–3208 (1965).
[5] G. Reecht, B.W. Heinrich, H. Bulou, F. Scheurer, L. Limot, and G. Schull, New J. Phys. **19**(11), 113033 (2017).

[6] D. Pommier, R. Bretel, L.E.P. López, F. Fabre, A. Mayne, E. Boer-Duchemin, G. Dujardin, G. Schull, S. Berciaud, and E. Le Moal, Phys. Rev. Lett. **123**(2), 027402 (2019).
[7] Y. Zhang, Y. Luo, Y. Zhang, Y.-J. Yu, Y.-M. Kuang, L. Zhang, Q.-S. Meng, Y. Luo, J.-L. Yang, Z.-C. Dong, and J.G. Hou, Nature **531**(7596), 623–627 (2016).
[8] J. Aizpurua, S.P. Apell, and R. Berndt, Phys. Rev. B **62**(3), 2065–2073 (2000).
[9] Y. Zhang, Q.-S. Meng, L. Zhang, Y. Luo, Y.-J. Yu, B. Yang, Y. Zhang, R. Esteban, J. Aizpurua, Y. Luo, J.-L. Yang, Z.-C. Dong, and J.G. Hou, Nat Commun **8**(1), 15225 (2017).
[10] L. Zhang, Y.-J. Yu, L.-G. Chen, Y. Luo, B. Yang, F.-F. Kong, G. Chen, Y. Zhang, Q. Zhang, Y. Luo, J.-L. Yang, Z.-C. Dong, and J.G. Hou, Nat Commun **8**(1), 580 (2017).
[11] Y. Luo, G. Chen, Y. Zhang, L. Zhang, Y. Yu, F. Kong, X. Tian, Y. Zhang, C. Shan, Y. Luo, J. Yang, V. Sandoghdar, Z. Dong, and J.G. Hou, Phys. Rev. Lett. **122**(23), 233901 (2019).
[12] J. Kröger, B. Doppagne, F. Scheurer, and G. Schull, Nano Lett. **18**(6), 3407–3413 (2018).
[13] M. Lelek, M.T. Gyparaki, G. Beliu, F. Schueder, J. Griffié, S. Manley, R. Jungmann, M. Sauer, M. Lakadamyali, and C. Zimmer, Nat Rev Methods Primers **1**(1), 1–27 (2021).
[14] J. Doležal, S. Canola, P. Hapala, R.C. de Campos Ferreira, P. Merino, and M. Švec, ACS Nano **16**(1), 1082–1088 (2022).
[15] I. Zoh, M. Imai-Imada, J. Bae, H. Imada, Y. Tsuchiya, C. Adachi, and Y. Kim, J. Phys. Chem. Lett. **12**(31), 7512–7518 (2021).
[16] M. Imai-Imada, H. Imada, K. Miwa, Y. Tanaka, K. Kimura, I. Zoh, R.B. Jaculbia, H. Yoshino, A. Muranaka, M. Uchiyama, and Y. Kim, Nature **603**(7903), 829–834 (2022).
[17] Q. Meng, C. Zhang, Y. Zhang, Y. Zhang, Y. Liao, and Z. Dong, Applied Physics Letters **107**(4), 043103 (2015).
[18] M.C. Chong, L. Sosa-Vargas, H. Bulou, A. Boeglin, F. Scheurer, F. Mathevet, and G. Schull, Nano Lett. **16**(10), 6480–6484 (2016).
[19] T. Neuman, R. Esteban, D. Casanova, F.J. García-Vidal, and J. Aizpurua, Nano Lett. **18**(4), 2358–2364 (2018).
[20] Y. Zhang, Z.C. Dong, and J. Aizpurua, Journal of Physical Chemistry C **124**(8), 4674–4683 (2020).
[21] G. Rosolen, and B. Maes, APL Photonics **6**(8), 1–9 (2021).
[22] S. Smeets, B. Maes, and G. Rosolen, Phys. Rev. A **107**(6), 063516 (2023).
[23] A. Rosławska, T. Neuman, B. Doppagne, A.G. Borisov, M. Romeo, F. Scheurer, J. Aizpurua, and G. Schull, Phys. Rev. X **12**(1), 011012 (2022).
[24] S. Lyu, Y. Zhang, Y. Zhang, K. Chang, G. Zheng, and L. Wang, J. Phys. Chem. C **126**(27), 11129–11137 (2022).
[25] A.G. Borisov, F. Aguillon, and D.C. Marinica, Journal of Physical Chemistry C **124**(51), 28210–28219 (2020).
[26] M. Romanelli, G. Dall'Osto, and S. Corni, The Journal of Chemical Physics **155**(21), 214304 (2021).
[27] C.V. Coane, M. Romanelli, G. Dall'Osto, R. Di Felice, and S. Corni, Commun Chem **7**(1), 1–11 (2024).
[28] J. Flick, N. Rivera, and P. Narang, Nanophotonics **7**(9), 1479–1501 (2018).
[29] P. Forn-Díaz, L. Lamata, E. Rico, J. Kono, and E. Solano, Reviews of Modern Physics **91**(2), (2019).
[30] T.E. Li, B. Cui, J.E. Subotnik, and A. Nitzan, Annual Review of Physical Chemistry **73**, 43–71 (2021).
[31] L. Novotny, and B. Hecht, *Principles of Nano-Optics*, 2nd ed. (Cambridge University Press, Cambridge, 2012).
[32] J.J. Sakurai, and J. Napolitano, *Modern Quantum Mechanics*, Third edition (Cambridge University Press, Cambridge, 2020).
[33] A.F. Koenderink, ACS Photonics **4**(4), 710–722 (2017).
[34] N. Rivera, I. Kaminer, B. Zhen, J.D. Joannopoulos, and M. Soljačić, Science **353**(6296), 263–269 (2016).
[35] H. Meier, U. Stalmach, and H. Kolshorn, Acta Polymerica **48**(9), 379–384 (1997).
[36] N. Takeshima, K. Sugawa, H. Tahara, S. Jin, H. Wakui, M. Fukushima, K. Tokuda, S. Igari, K. Kanakubo, Y. Hayakawa, R. Katoh, K. Takase, and J. Otsuki, ACS Nano **13**(11), 13244–13256 (2019).
[37] M. Ans, K. Ayub, X. Xiao, and J. Iqbal, Journal of Molecular Liquids **298**, 111963 (2020).

[38] M.C. Chong, N. Afshar-Imani, F. Scheurer, C. Cardoso, A. Ferretti, D. Prezzi, and G. Schull, Nano Lett. **18**(1), 175–181 (2018).
[39] A.D. Laurent, and D. Jacquemin, International Journal of Quantum Chemistry **113**(17), 2019–2039 (2013).
[40] P.Y. Chen, D.J. Bergman, and Y. Sivan, Phys. Rev. Appl. **11**(4), 044018 (2019).
[41] G. Rosolen, B. Maes, P.Y. Chen, and Y. Sivan, Phys. Rev. B **101**(15), 155401 (2020).
[42] P. Lalanne, W. Yan, K. Vynck, C. Sauvan, and J.-P. Hugonin, Laser & Photonics Reviews **12**(5), 1700113 (2018).
[43] D.J. Bergman, and D. Stroud, Phys. Rev. B **22**(8), 3527–3539 (1980).
[44] K.A. Michalski, and M.M. Mustafa, Journal of Applied Physics **125**(5), 055302 (2019).
[45] P.O. Löwdin, Physical Review **97**(6), 1474–1489 (1955).
[46] F. Furche, The Journal of Chemical Physics **114**(14), 5982–5992 (2001).
[47] T. Etienne, Journal of Chemical Physics **142**(24), (2015).
[48] Y. Li, and C.A. Ullrich, Chemical Physics **391**(1), 157–163 (2011).
[49] R.L. Martin, Journal of Chemical Physics **118**(11), 4775–4777 (2003).
[50] T. Yanai, D.P. Tew, and N.C. Handy, Chemical Physics Letters **393**(1), 51–57 (2004).
[51](N.d.).
[52] P.B. Johnson, and R.W. Christy, Phys. Rev. B **6**(12), 4370–4379 (1972).
[53] B. Yang, G. Chen, A. Ghafoor, Y. Zhang, Y. Zhang, Y. Zhang, Y. Luo, J. Yang, V. Sandoghdar, J. Aizpurua, Z. Dong, and J.G. Hou, Nat. Photonics **14**(11), 693–699 (2020).
[54] M. Urbieta, M. Barbry, Y. Zhang, P. Koval, D. Sánchez-Portal, N. Zabala, and J. Aizpurua, ACS Nano **12**(1), 585–595 (2018).
[55] N. Kazemi-Zanjani, S. Vedraine, and F. Lagugné-Labarthet, Opt. Express, OE **21**(21), 25271–25276 (2013).
[56] P. Anger, P. Bharadwaj, and L. Novotny, Phys. Rev. Lett. **96**(11), 113002 (2006).
[57] M.L. Andersen, S. Stobbe, A.S. Sørensen, and P. Lodahl, Nature Phys **7**(3), 215–218 (2011).
[58] L. Novotny, J. Opt. Soc. Am. B, JOSAB **19**(6), 1355–1362 (2002).
[59] P. Tighineanu, M.L. Andersen, A.S. Sørensen, S. Stobbe, and P. Lodahl, Phys. Rev. Lett. **113**(4), 043601 (2014).
[60] E. Rusak, J. Straubel, P. Gładysz, M. Göddel, A. Kędziorski, M. Kühn, F. Weigend, C. Rockstuhl, and K. Słowik, Nat Commun **10**(1), 5775 (2019).